On the structural origin of the anisotropy in the myocardium: Multiscale modeling and analysis

Nicole Tueni, Jean-Marc Allain, Martin Genet

On the structural origin of the anisotropy in the myocardium: Multiscale modeling and analysis

Nicole Tueni[a,b], Jean-Marc Allain[a,b], Martin Genet[a,b]
[a]LMS, CNRS/École Polytechnique/
Institut Polytechnique de Paris, Palaiseau, France
[b]Inria, Palaiseau, France

February 16, 2022

Abstract

Due to structural heterogeneities within the tissue, the myocardium displays an orthotropic material behavior. However, the link between the microstructure and the macroscopic mechanical properties is still not fully established. In particular, if it is admitted that the cardiomyocyte organization induces a transversely isotropic symmetry, the relative role in the observed orthotropic symmetry of cardiomyocyte orientation variation and perimysium collagen "sheetlet" structure, two mechanisms occurring at different scales, is still a matter of debate. In order to shed light on this question, we designed a multiscale model of the myocardium, bridging the cell, sheetlet and tissue scales. More precisely, we compared the macroscopic anisotropy obtained by homogenization of different mesostructures consisting in cardiomyocytes and extracellular collageneous layers, also taking into account the variation of cardiomyocyte and sheetlet orientations on the macroscale, to available experimental data. This study confirms the importance of sheetlets layers in assuring the tissue's anisotropic response, as cardiomyocytes-only mesostructures cannot reproduce the observed anisotropy. Moreover, our model shows the existence of a size effect in the myocardial tissue shear properties, which will require further experimental analysis.

Contents

1 Introduction

The cardiac tissue has a highly complex multiscale architecture that can be decomposed into three main scales: the cell scale (10-100 µm), the sheetlet scale (100-1000 µm), and the tissue scale (1-10 mm) [Hunter, 1975]. At the cellular scale, the cardiomyocytes are roughly cylindrical, measuring 100-150 µm by 10-20 µm, surrounded by a thin layer of connective tissue, called endomysium. The cardiomyocytes are locally parallel, arranged in bundles or fascicles of 5 to 10 cells, forming structures of 100-200 µm, wrapped by a perimysial layer of extracellular collagen called "sheetlets". At the tissue scale, the cardiomyocyte orientation has been widely studied: the myocardial fiber orientation exhibits a helical geometry, characterized by the Helical Angle (HA), that transitions continuously and smoothly through the cardiac wall from about $+60°$ close to the endocardium to about $-60°$ at the epicardium in the human heart [Streeter and Bassett, 1966; Streeter et al., 1969]. However, it is still unclear how the sheetlets are organized through the myocardial thickness, and along its wall: while some studies support the predominance of a single laminar sheetlet population, with an orientation that evolves linearly from about $-90°$ near the endocardium to about $+90°$ near the epicardium [LeGrice et al., 1995; Ferreira et al., 2014; Nielles-Vallespin et al., 2017], other studies propose the coexistence of two local myocardial sheet populations [Kung et al., 2011; Kilner et al., 2015].

Knowledge about the passive mechanical properties of the cardiac tissue has evolved over time. Various constitutive models of the passive properties of the myocardium have been proposed in the past few decades, which can be split into two categories. The first one includes macroscopic models that comprise (i) phenomenological models based on general observations of the material symmetries and orientations in the tissue [Demiray, 1976; Guccione et al., 1991] and (ii) structure-based models that take into account quantitative information about each constituent in the myocardium [Horowitz et al., 1988; Holzapfel and Ogden, 2009]. The second one consists in microstructure-based Representative Volume Element (RVE) models, where the RVE include a selection of microstructural heterogeneities [McEvoy et al., 2018]. Phenomenological models of the myocardium are the most common in the literature. Several of the simplest models are based on isotropic elasticity [Demiray, 1976]. Early invariant-based macroscopic models suppose that the tissue is transversely isotropic, with one preferred direction in the myocardium, the fiber orientation [Humphrey and Yin, 1987]. Other models have been proposed over the years; however, it became more and more clear that the passive behavior could not be fully described by a transversely isotropic model. Thus, macroscopic orthotropic models were also developed [Guccione et al., 1991; Costa et al., 2001].

One breakthrough experiment performed by [Dokos et al., 2002] implemented shear tests to study the anisotropic response of the myocardium. Simple shear was applied to cubic myocardium samples extracted from porcine hearts with respect to the three principal material axes (the fiber axis (F), the sheetlet axis (S) and the normal to the fiber-sheetlet plane (N)) in six shear modes. It resulted in six different forces, highlighting the anisotropy in the tissue. The

deformation that produced an extension of the cardiac fibers (FS, FN) resulted in the highest resistance to shear, and the ones producing an extension in the normal to sheetlet direction (NF, NS) resulted in the lowest resistance to shear. Similar results were later obtained for human hearts [Sommer et al., 2015]. More orthotropic models were thus developed [Schmid et al., 2006, 2008]. More recently, [Holzapfel and Ogden, 2009] proposed a model considering the fiber (f), the sheetlet (s) and the sheet-normal (n) directions in the tissue. Although these models give a fairly good description of the macroscopic mechanical properties of the cardiac tissue, they lack explicit microstructural information, hence cannot fully account for microstructural features and microscopic deformation mechanisms. In order to do so, models containing quantitative information about the composition and microstructure of the myocardium should be developed.

Structure-based models take into account detailed structural information about the tissue constituents, separating their mechanical contributions, and accounting for the interactions between them [Horowitz et al., 1988; Humphrey and Yin, 1989]. Relatively recent structure-based models have been developed [Avazmohammadi et al., 2017], using histological images to quantify the orientation distributions and volume fraction of the cardiomyocytes, collagen fibers and amorphous ground matrix. The energy contributions take into account the orientation distribution of each of the constituents. Although promising, structure-based models are complex, as they contain a large number of parameters that require microstructural parameters difficult to obtain. Moreover, existing models focus on the microstructure at the cellular scale, and do not straightforwardly represent the sheetlet scale.

Micromechanical modeling consists in identifying an heterogeneous RVE and specifying proper mechanical properties for each constituents in order to study local deformation mechanisms and global response. This allows notably to generate the resulting properties of the material at the upper spatial scale. Micromechanical models for the cardiac tissue are sparse, probably due to the complexity of the tissue organization, and to the difficulty in identifying a suitable RVE. The work of [McEvoy et al., 2018] proposed a microstructural model of the myocardium, generating an RVE based on histological studies, containing layers of parallel cardiomyocytes, surrounded by a layer of endomysium (ECM 1) comprising vasculature. The layers are separated by perimysial collagen (ECM 2). Collagen and cardiomyocytes are represented by a compressible hyperelastic model [Nolan et al., 2014] that takes into account the collagen fiber dispersion. The presence of an underlying isotropic material is also supposed, and is described by a neo-hookean model. In order to investigate the compressibility of the myocardium, the RVE is subjected to confined compression and shows that at an applied strain of 5%, the vasculature volume decreases by 6.2%, ECM 1 by 6.98%, ECM 2 by 6.2% and the cardiomyocytes by 0.5%. Moreover, under such loading, all the fibers shorten, and the stress is governed by the isotropic elastic behavior of the cardiomyocytes and extracellular matrix. Six modes of shear deformation are then applied to the RVE. The obtained shear behavior corresponds to the ones obtained previously by [Dokos et al., 2002; Sommer et al., 2015], with both the shear stiffening and the correct order in the

stresses (FS>FN≥SF>SN>NF≅NS). The non-linear responses to shear in NS and NF are shown to be dependent on the endomysial and perimysial collagen dispersion. The shear responses in SN and SF are also due to the perimysial fibers aligned with the sheetlet direction, and the high stresses observed in FS and FN are caused by the cardiomyocytes, with a higher stress for FS due to the dispersion of the perimysial extracellular matrix. To our knowledge, this is the only micromechanical model that takes into account the microstructural information of the cardiac tissue, and reproduces its macroscopic anisotropy; however, it does not pinpoint the structural component that induces this anisotropy at the macroscale.

The anisotropic response of the cardiac tissue arises from two structural arrangements in the tissue: the transmural variation of the cardiomyocyte orientation (typically $\pm 60^\circ$ in humans), and the configuration of the perimysial extracellular matrix surrounding the cardiomyocyte bundles in sheetlets. However, no study has been conducted yet to assess to what extent each of these structures, which occur at different scales, contribute to the observed macroscopic anisotropy. To address this question, experimental approaches require to manipulate very small samples, and have not been performed up to now to our best knowledge. Thus, in this study, we propose a multiscale model (see Section 2.1) of the myocardium bridging the cell, sheetlet and tissue scales, and aiming at determining the structural origin of the observed macroscale mechanical anisotropy by [Dokos et al., 2002] (see Section 2.2). Various mesostructures are considered (see Section 2.1.1) and homogenized (see Section 2.1.3), the resulting behavior being used in a macroscopic model of the experimental setup (see Section 2.2.2). An optimization procedure (see Section 2.3) allows to identify mesoscopic parameters minimizing the discrepancy between the macroscopic anisotropies predicted by the model and observed experimentally, thus permitting to determine which mesostructure is potentially compatible with the experimental data and which is not.

2 Materials and methods

A global schematic of our analysis is shown in Figure 1. To accurately represent the cardiac hierarchical architecture, we took advantage of the tissue scale separation: at the mesoscopic scale (100-500 μm), we explored structures made of cardiac cells and extracellular matrix with homogeneous orientation of the fibers (see Section 2.1.1). Given the mesostructure, and a set of material parameters $\underline{p}$ verifying thermodynamic bounds (see Section 2.1.2), periodic homogenization was performed (see Section 2.1.3), generating the homogenized material properties of the resulting medium $\left\langle \underline{\underline{\underline{\underline{C}}}} \right\rangle$. These properties were then used at the macroscale (>1 mm), where we took into account the change in orientation of the mesostructure (see Section), and the experimental tests were simulated (see Section 2.2.2). The obtained numerical results were compared to the experimental ones using a cost function to optimize the microstructural parameters

(see Section 2.3). We will now detail each step of the analysis.

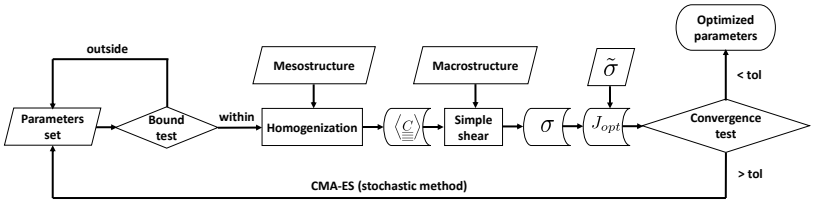

Figure 1: Schematic representation of the adopted method: given a mesostructure and a set of material parameters respecting the elastic bounds, a linear homogenization is performed, generating the homogenized stiffness matrix $\left\langle \underline{\underline{\underline{\underline{C}}}} \right\rangle$ of the resulting medium. These properties are used at the macroscale to simulate the experimental shear tests. The obtained numerical stresses $\underline{\underline{\sigma}}$ are compared to experimental ones $\tilde{\underline{\underline{\sigma}}}$ via a cost function J_{opt}. A stochastic, derivative-free method is used to identify mesoscopic parameters that minimize the cost function.

2.1 Mesoscopic modeling and upscaling

We explored three mesostructures (see Figure 2, Mesoscale): first, a homogeneous mesostructure (H), made only of cardiomyocytes, aligned with the direction $\underline{f}$. Then a second mesostructure (L), made of two blocks of cardiomyocytes aligned with $\underline{f}$, separated by a plane layer of extracellular matrix. Finally a third mesostructure, (E), made of cardiac cells aligned with $\underline{f}$, separated by the collagen layer forming an ellipsoid.

2.1.1 Mesostructures

Structure H: Homogeneous. As already mentioned, the first "mesostructure" is actually homogeneous, made of cardiomyocytes wrapped by endomysial collagen. This structure was considered to determine whether the cardiomyocyte rotation can explain alone the observed anisotropy at the macroscale.

Structure L: Laminar. This mesostructure was considered in order to investigate the effect of a laminar structure for the myocardium on the orthotropy [LeGrice et al., 1995; Young et al., 1998; Sands et al., 2005; Pope et al., 2008]. The structure was made of two blocks (50 μm) of parallel cardiac cells each wrapped by endomysial collagen, separated by a layer of perimysial extracellular matrix. It has been shown that the collagen content of the heart evolves with age: while it is of 3.92± 0.8% in young subjects, it reaches 5.86± 0.81% in old hearts [Debessa et al., 2001]. We fixed the collagen thickness layer to 5 μm, representing 4.75% of the total volume.

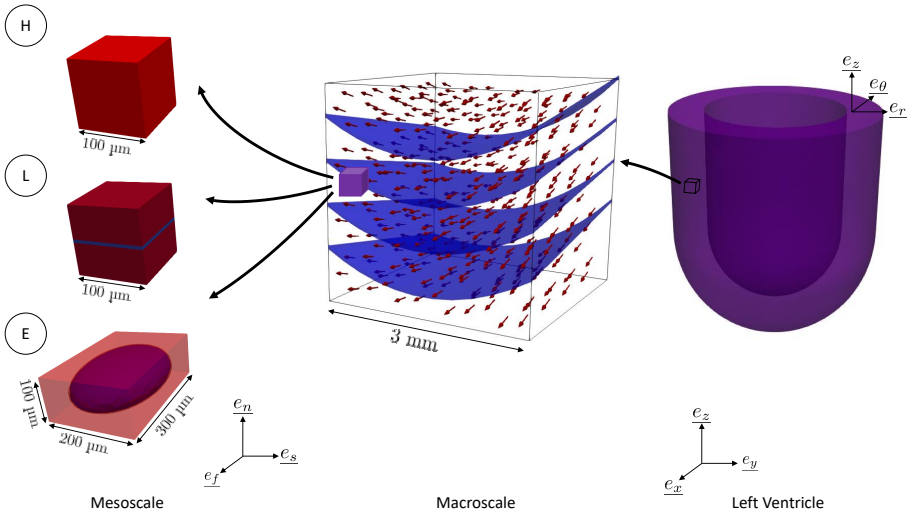

Figure 2: Schematic showing the different scales for the mesoscale. We tested 3 different structures (H, L and E), where the cardiomyocytes wrapped by endomysium are represented in red, and perimysium in blue. The macroscale shows the orientation evolution of the cardiac cells and sheetlets in a 3×3×3 mm cubic sample, similar to the ones used experimentally.

Structure E: Ellipsoidal. This mesostructure was explored in order to investigate the effect of the ellipsoidal clusters observed in the cross-sections of the cardiac wall [Kanzaki et al., 2010]. We created an ellipsoid such that it has 3 different axis ratios in the 3 different planes (see Figure 3) in order to avoid having a transversely isotropic structure. Hence, our cell dimensions were 100×200×300 μm. The extracellular matrix layer thickness was 2.5 μm, representing 4.79% of the total volume.

2.1.2 Mesoscopic behavior and bounds on material parameters

In the following, we introduce the constitutive law for both cardiomyocytes and extracellular matrix. We also recall the elastic bound, for compressible [Lempriere, 1968], and incompressible [Loredo and Klöcker, 1997; Garcia et al., 1998] materials.

Cardiomyocytes. The cardiomyocytes being cylindrical elongated cells, it is thus natural to model them as a transversely isotropic material, with physical properties symmetric about the cell axis ($\underline{e_f}$). The bundles being made of locally parallel cells, they are also transversely isotropic. The material parameters for the cardiomyocytes are therefore: E_f, the longitudinal elastic modulus, E_t, the transverse or in-plane elastic modulus, G_{tt} and ν_{tt}, the in-plane shear modulus and Poisson ratio and G_{ft} and ν_{ft}, the transverse shear modulus and

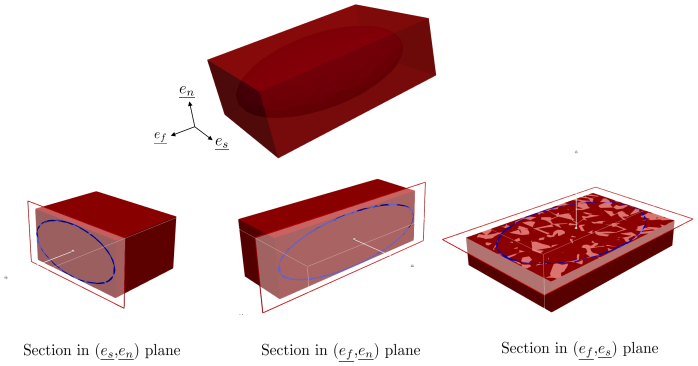

Figure 3: Complete structure E and sections showing the different ellipse ratios on in three orthogonal planes, in order to create an orthotropic mesostructure.

the Poisson ratio. The myocardial volume change (up to 10%) during the cardiac cycle, is partly caused by the cardiac structure [Ashikaga et al., 2008]. We therefore considered two cases for the cardiomyocytes: compressible and quasi-incompressible. Bounds on elastic constants for a transversely isotropic material are recalled in Table 1.

Compressible material	Incompressible material
$E_f > 0$	$E_f > 0$
$E_t > 0$	$E_t > 0$
$G_{ft} > 0$	$G_{ft} > 0$
$G_{tt} = \frac{E_t}{2(1+\nu_{tt})}$	$G_{tt} = \frac{E_f E_t}{4E_f - E_t}$
$-\sqrt{\frac{E_f}{E_t}} < \nu_{ft} < \sqrt{\frac{E_f}{E_t}}$	$\nu_{ft} = 0.5$
$-1 < \nu_{tt} < 1 - 2\nu_{ft}^2 \frac{E_t}{E_f}$	$\nu_{tt} = 1 - \frac{E_t}{2E_f}$
	$E_f > \frac{E_t}{4}$

Table 1: Elastic bounds for a compressible (left) and incompressible (right) transversely isotropic material.

Collagen layers. The choice of constitutive law for the extracellular matrix is not straightforward. Indeed, it is a thin layer made mostly of interlocking collagen fibers arranged randomly. This structure hints at a transversely isotropic symmetry, with uniform parameters in the plane, and a symmetry axis orthogonal to the plane. This leads to six material parameters. Considering the thinness of the layer, these parameters might not be identifiable, as confirmed by our sensitivity analysis in Appendix B. Thus, we use an isotropic material to the extracellular matrix, with only two parameters to identify: the elastic

modulus E_c (always > 0), and the Poisson ratio ν_c comprised between -1 and 0.5.

2.1.3 Periodic homogenization

The cardiac tissue being made of different constituents, its homogenized mechanical properties at the macroscale will depend on the coefficients of the different constituents. Initially, homogenization techniques were based on the Hill-Mandel lemma which separates the material into two scales, and connects the mechanical energies of both scales [Hill, 1963]. Later developments showed that the result can be recovered using a two-scale expansion method [Sanchez-Palencia, 1974; Michel et al., 1999]. In our study, the two scales consist of the mesoscale and the macroscale: At the mesoscale, the periodic unit cell (Ω) (mesostructures (L) and (E)) is heterogeneous, made of two materials, cardiomyocytes and collageneous extracellular matrix. In order to obtain the material properties of the homogeneous medium associated with each of the mesostructures, periodic homogenization was performed numerically, and allowed to compute the homogenized elasticity tensor $\left\langle \underline{\underline{\underline{\underline{C}}}} \right\rangle$ at the mesoscale. All finite element computations were performed using the FEniCS library [Alnæs et al., 2015].

2.2 Experimental data and associated modeling at macroscale

2.2.1 Shear experiments and anisotropy characterization

Experiments revealing the anisotropic nature of the cardiac tissue consisted in applying cycles of sinusoidal simple shear, during which the maximum shear strain was increased, at each cycle between 5% and 50%, in six shear modes NS, NF, FN, FS, SF, SN, on 3×3×3 mm cubic porcine samples [Dokos et al., 2002], and 4×4×4 mm cubic human samples [Sommer et al., 2015]. Both studies reveal the material anisotropy with a difference in the shear stresses along the six directions, with the highest values for the FS and FN modes, and the lowest ones for the NF and NS modes (see Figure 13 in Appendix A).

We conducted our study using the data sent to us by Prof. Socrates Dokos [Dokos et al., 2002]. We plotted the recorded stresses at 5%, 10%, 20%, 30%, 40% and 50% shear deformation for all modes (see Figure 4). We noticed that the mode order stays consistent for all deformation levels, with the highest stresses recorded for FS, followed by FN, SF, SN, NF and finally NS. We therefore concluded that the anisotropy is inherent to the material, and not induced by large deformations. Thus, in order to investigate the structural origin of tissue anisotropy, the small deformations mechanical framework is sufficient.

2.2.2 Associated macroscopic model

We simulated a 3×3×3 mm cube as seen in the experiment (see Figure 2, Macroscale). The cardiac fibers and the sheetlets rotate in the cardiac tissue.

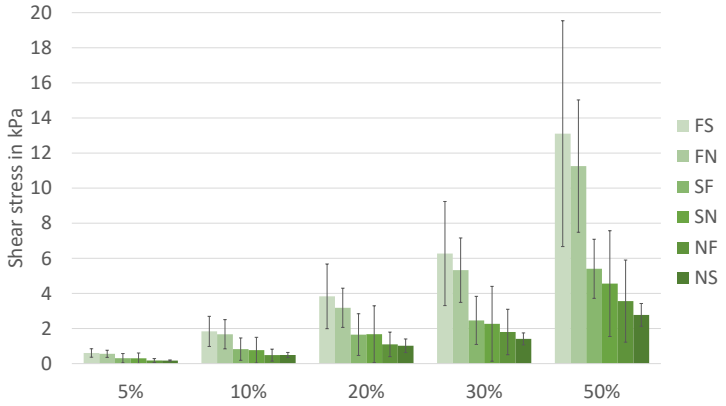

Figure 4: Shear stress recorded at 5%, 10%, 20%, 30%, 40% and 50% deformation for all modes showing a conservation of the anisotropy for small and large deformations. Data obtained from [Dokos et al., 2002].

We therefore reproduced this rotation in our numerical cube. The cardiac fibers rotate along $\underline{e_r}$ by an angle α, in the $(\underline{e_\theta}, \underline{e_z})$ plane. This leads to the rotation of $\underline{e_z}$ around $\underline{e_\theta}$ of an angle α as well, creating a new local system $(\underline{e_r}, \underline{e_f}, \underline{e'_z})$. The sheetlets rotate around e_f by an angle β, leading to a rotation of $\underline{e'_z}$ in this same plane, of an angle β. The new local coordinate system for fibers, sheetlets, and normal to fiber-sheetlets orientations become $(\underline{e_f}, \underline{e_s}, \underline{e_n})$, as illustrated in Figure 5.

Fiber orientation. Cardiomyocytes rotate in the cardiac wall, from endocardium to epicardium, such that they constitute a helical structure. Their orientation is called the Helix Angle (HA), and varies linearly between +60° to –60° in heart walls (10 mm) [Streeter and Bassett, 1966; Streeter et al., 1969]. Considering that the samples are extracted from mid wall, we assumed that the fiber orientation α varies linearly between +18° to –18°.

Sheetlet orientation. The sheetlet orientation distribution in the cardiac wall has not been fully characterized yet. Although this question has attracted more and more attention, disparities between the observations and the lack of a clear mapping of the sheetlets in the left ventricle leave this question partially unanswered [LeGrice et al., 1995; Rohmer et al., 2007; Kung et al., 2011; Nielles-Vallespin et al., 2017]. Cross-sections, orthogonal to the cardiomyocytes, have shown an important variation of the sheetlet orientation (β) along the slices, ranging from –90° to +90°. However, disparities in the values between the different studies indicate that this orientation is still not fully understood. We thus decided to conduct this study for several sheetlet orientations, ranging from ±0° to ±50° from endocardium to epicardium, hence analyzing the effect of their orientation on the tissue's macroscopic behavior.

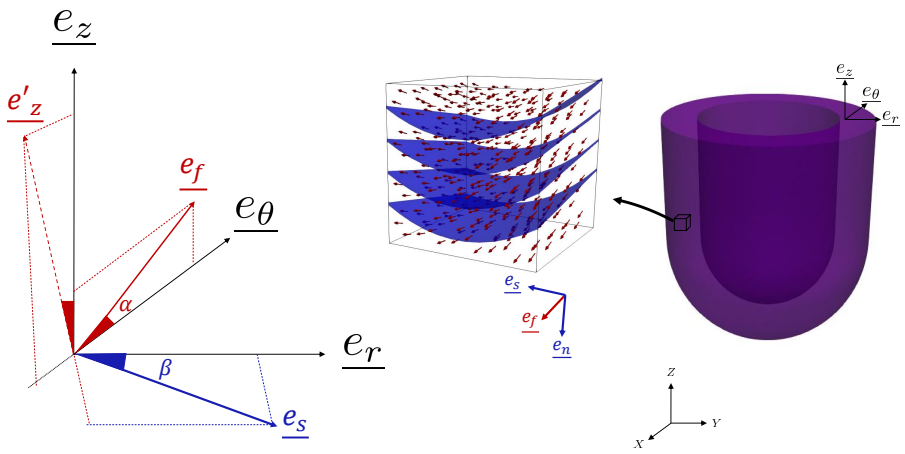

Figure 5: Euler angles representing rotation of local fiber and sheetlet system with respect to global basis. In red: rotation of of angle α along $\underline{e_r}$, leading to new system $(\underline{e_r}, \underline{e_f}, \underline{e'_z})$. In blue: rotation of $\underline{e_r}$ around $\underline{e_f}$ by angle β in $(\underline{e_r}, \underline{e'_z})$ plane, creating the new local system $(\underline{e_f}, \underline{e_s}, \underline{e_n})$. Cardiomyocytes are aligned with $\underline{e_f}$, and sheetlets are in the $(\underline{e_f}, \underline{e_s})$ plane.

Material parameters. The homogenized stiffness matrix $\left\langle \underline{\underline{\underline{\underline{C}}}} \right\rangle$, computed in Section 2.1.3, was used as an input material parameter at the macroscale. It was oriented with the $(\underline{e_f}, \underline{e_s}, \underline{e_n})$ basis at every point of the macrostructure.

Simple shear. Simple shear tests were simulated: Dirichlet boundary conditions were applied on two sides of the cube, as shown in Figure 6, while keeping the others stress-free. We restricted our problem to the linear elastic behavior. Thus, the problem consisted in finding the displacement $\underline{u}(\underline{p})$ such that:

$$\begin{cases} \underline{\nabla}(\underline{\sigma}) = \underline{0}, \quad \underline{\underline{\sigma}} = \underline{\underline{\sigma}}^{\mathrm{T}} & \text{in } \Omega \\ \underline{\underline{\sigma}} = \left\langle \underline{\underline{\underline{\underline{C}}}} \right\rangle : \underline{\underline{\epsilon}} & \text{in } \Omega \\ \underline{\underline{\epsilon}} = \frac{1}{2}(\underline{\underline{\nabla}}(\underline{u}) + (\underline{\underline{\nabla}}(\underline{u}))^T) & \text{in } \Omega \end{cases}$$

The solution $\underline{u}(\underline{p})$ to the problem allowed to compute the resultant shear stress $\underline{\underline{\sigma}}(\underline{p})$ for each of the six different sets of Dirichlet boundary conditions (see Table2).

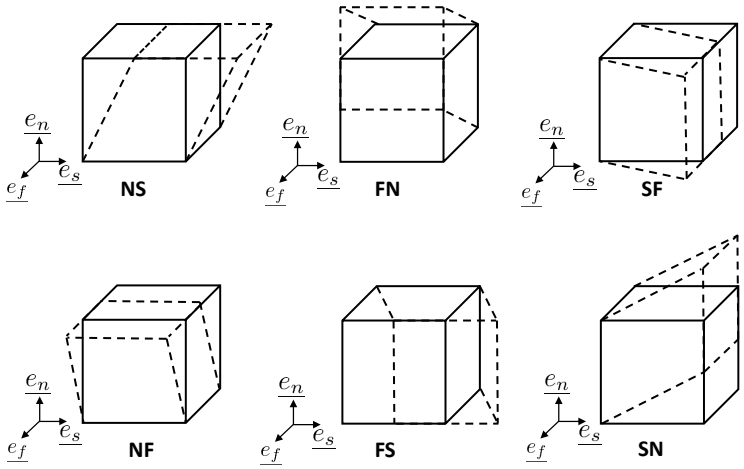

Figure 6: Schematic showing six possible simple shear modes for an orthotropic myocardium cube defined with respect to the fiber (f), sheet (s), and sheet-normal (n) directions. Replicated from [Dokos et al., 2002].

FN mode	$u(x_1 = 0) = [0, 0, 0]$	$u(x_1 = 3) = [0, 0, \bar{u}]$
FS mode	$u(x_1 = 0) = [0, 0, 0]$	$u(x_1 = 3) = [0, \bar{u}, 0]$
SF mode	$u(x_2 = 0) = [0, 0, 0]$	$u(x_2 = 3) = [\bar{u}, 0, 0]$
SN mode	$u(x_2 = 0) = [0, 0, 0]$	$u(x_2 = 3) = [0, 0, \bar{u}]$
NS mode	$u(x_3 = 0) = [0, 0, 0]$	$u(x_3 = 3) = [0, \bar{u}, 0]$
NF mode	$u(x_3 = 0) = [0, 0, 0]$	$u(x_3 = 3) = [\bar{u}, 0, 0]$

Table 2: Dirichlet boundary conditions applied on the macroscopic cube in 6 modes

2.3 Sensitivity analysis and parameter optimization

2.3.1 Material parameter sensitivity

Prior to performing the material parameter estimation, a sensitivity analysis was conducted to identify the parameters identifiability at the mesoscale, with the parameters influence on the homogenized material properties, and at the macroscale, with their influence on the macroscopic shear response. The sensitivity analysis method and results are presented in Appendix B. The main results show that the responses at both scales are not sensitive to the extracellular collageneous material parameters, which is due to its low volume fraction in the tissue. As a consequence, we decided to use an isotropic material for this layer (see Section 2.1.2), and we fixed its corresponding Young modulus E_c and Poisson ratio ν_c.

2.3.2 Parameter estimation

Given that (i) our model is linear (hence the stress depends linearly on the stiffness), and (ii) our main objective was to compare the anisotropy (or the order of the shear stresses), we fixed one microscopic Young modulus ($E_t = 1$ $a.u.$) and actually considered shear stress ratios instead of the stresses themselves in the cost function. The experimental stress ratios $\tilde{R}$ and numerical ratios R were $\{\frac{\tilde{\sigma}_{FN}}{\tilde{\sigma}_{FS}}, \frac{\tilde{\sigma}_{SF}}{\tilde{\sigma}_{FS}}, \frac{\tilde{\sigma}_{SN}}{\tilde{\sigma}_{FS}}, \frac{\tilde{\sigma}_{NS}}{\tilde{\sigma}_{FS}}, \frac{\tilde{\sigma}_{NF}}{\tilde{\sigma}_{FS}}\}$ and $\{\frac{\sigma_{FN}}{\sigma_{FS}}, \frac{\sigma_{SF}}{\sigma_{FS}}, \frac{\sigma_{SN}}{\sigma_{FS}}, \frac{\sigma_{NS}}{\sigma_{FS}}, \frac{\sigma_{NF}}{\sigma_{FS}}\}$, respectively. The optimization cost function J_{opt} was

$$J_{opt} = \sum_{i=1}^{5} \frac{(R_i - \mu_{\tilde{R}_i})^2}{s^2_{\tilde{R}_i}}, \tag{2.1}$$

$\mu_{\tilde{R}_i}$ being the mean value of ratio $\tilde{R}_i$, and $s_{\tilde{R}_i}$ its standard deviation, given that each experiment is repeated on six specimen. The parameter optimization was performed using CMA-ES (Covariance Matrix Adaptation-Evolution Strategy), which uses stochastic, derivative-free methods for numerical optimization [Igel et al., 2006].

2.4 Size effect

In order to investigate the size effect on the anisotropy of the sample, we compared the shear stress ratios resulting from simple shear simulations on macroscopic cubes ranging from 1 to 10 mm. At the mesoscale, we chose to conduct the study with the mesostructure (L) and the optimized parameters that fit the experimental data. At the macroscale, as a reference, we simulated a linear variation of the cardiomyocyte orientation only, such that they vary between $\pm$ 6° for 1 mm samples and $\pm$ 60° for 10 mm samples. Then we added the evolution of the sheetlet orientation, such that β varies between $\pm$ 8.3° for 1 mm samples and $\pm$ 83.3° for 10 mm samples.

3 Results

We determined the optimal parameters for the different mesostructures (H), (L) and (E), and the different possible sheetlet angles (β), to determine which ones reproduce the best the experimental data.

3.1 Mesostructure (H)

Mesostructure (H) is made of aligned cardiomyocytes (see Figure 2, Mesoscale). This cell is already homogeneous; we therefore only simulated the simple shear displacement experiment on it and optimized the parameters.

A transversely isotropic material has six parameters (E_f, E_t, G_{ft}, G_{tt}, ν_{ft} & ν_{tt}) in the compressible case, while only four (E_f, E_t, G_{ft} & G_{tt}) in the incompressible case. We fixed one parameter, $E_t = 1$ *a.u.*, as we worked on the shear stress ratios, which left us with two parameters to optimize in the quasi-incompressible (E_f & G_{ft}), and four in the compressible (E_f, G_{ft}, ν_{ft} & ν_{tt}) cell (see Table 1).

Figure 7 shows bar plots of the optimized shear stress modes, superimposed with box plots of the experimental shear stress modes for compressible and quasi-incompressible cardiomyocytes. In both cases, the optimization cannot reproduce the experimental data, even though the results are slightly better in the compressible case, which has more degrees of freedom. By varying the parameters in order to recover the experimental order in the compressible mesostructure, we found that an increase in mode $\frac{SN}{FS}$ (c), led to an increase in mode $\frac{NF}{FS}$ (e) as well, change the order of the shear stress ratios. Their optimized values are shown in Table 3.

	Quasi-incompressible	Compressible
Optimized	$E_f = 2.07$ $G_{ft} = 28.29$	$E_f = 10.72$ $G_{ft} = 6.11$ $\nu_{ft} = 2.82$ $\nu_{tt} = -0.84$
Computed	$G_{tt} = 0.28$ $\nu_{tt} = 0.76$	$G_{tt} = 3.12$
Fixed	$E_t = 1$ $\nu_{ft} = 0.49$	$E_t = 1$

Table 3: Optimized cardiomyocyte material parameter ratios (normalized by $E_t = 1$) in the quasi-incompressible and compressible cases for mesostructure (H).

3.2 Mesostructure (L)

Mesostructure (L) is made of aligned cardiomyocytes separated by a planar layer of collagen. We consider the effect of the sheetlet angle (β) variation within the macroscale cube.

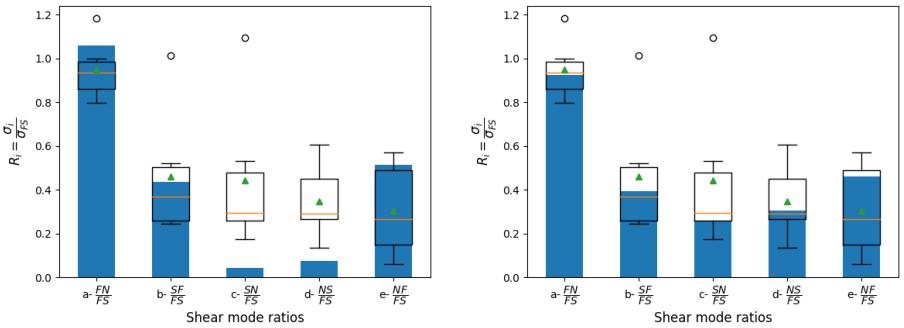

(a) Quasi-incompressible (b) Compressible

Figure 7: Experimental (box plot) *vs.* optimized (blue bar plot) shear stress ratios (normalized with respect to largest value) for the quasi-incompressible (left) and compressible (right) transversely isotropic Mesostructure (H). On the macroscale, we have $\alpha = \pm 18^\circ$ for all cases. Box plot: lower to upper quartile; whiskers: lowest datum above $Q_1 - 3 * (Q_3 - Q_1)/2$, and highest datum below $Q_1 + 3 * (Q_3 - Q_1)/2$, where Q_1 and Q_3 are the first and third quartiles; green triangle: mean; orange line: median; hollow circles: data points outside the whiskers. Data courtesy of Prof. Socrates Dokos [Dokos et al., 2002].

Quasi-incompressible cardiomyocytes. For quasi-incompressible cardiomyocytes, the experimental *vs.* numerical shear mode ratios are represented in Figure 8, for a sheetlet angle β varying between $\pm 0^\circ$, $\pm 12.5^\circ$, $\pm 25^\circ$, and $\pm 50^\circ$. The optimized parameters are shown in Table 4.

Even though the order of the optimized solutions agreed with the order of the experimental ratios, we were not able to find material parameters, within the bounds that match the experimental data (see Table 1). Optimized mode $\frac{SF}{FS}$ (b), was systematically too high compared to the experimental one for all values of β. We noticed, though, that the rotation of the sheetlets led to a closer solution. However, a rotation of the sheetlets of more then $\pm 50^\circ$ is unrealistic in a 3 mm cube, because it means that the sheetlets rotate of more than 300° in the cardiac wall, which is not physiological. Moreover, we concluded that the incompressibility hypothesis of the assembly of cardiomyocytes wrapped by endomysial extracellular matrix does not allow to reproduce the observed anisotropy at the macroscale.

Compressible cardiomyocytes. The optimized simulation *vs.* experimental data for compressible cardiomyocytes are shown in Figure 9. With the extra degree of freedom of the compressibility, we were able to match the experimental results. However, several optimal sets of parameters were obtained, meaning that the solution to this problem is not unique. This result indicates that it is not possible to identify many mesoscale parameters with simple shear assays at the macroscale. As seen previously, an increase in angle β leads to a better

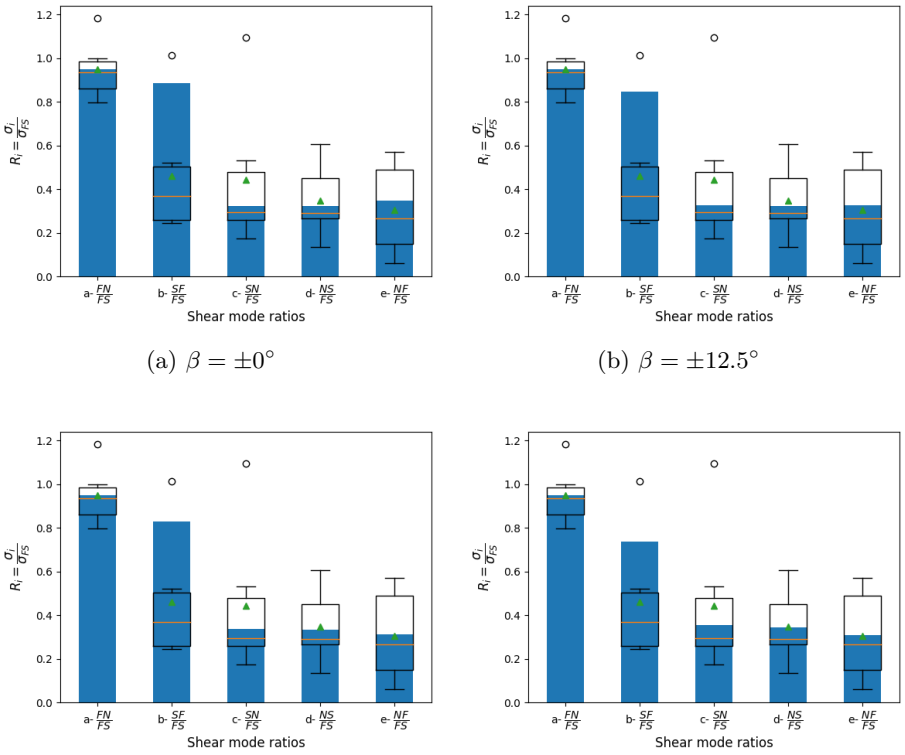

(a) $\beta = \pm 0°$ (b) $\beta = \pm 12.5°$

(c) $\beta = \pm 25°$ (d) $\beta = \pm 50°$

Figure 8: Quasi-incompressible cardiomyocytes in the laminar mesostructure (L), for $\alpha = \pm 18°$, with β ranging between $\pm 0°$ (a), $\pm 12.5°$ (b), $\pm 25°$ (c), $\pm 50°$ (d). See Figure 7 for details on box plots.

	$\pm 0°$	$\pm 12.5°$	$\pm 25°$	$\pm 50°$
Optimized	$E_f = 28.42$	$E_f = 28.73$	$E_f = 29.36$	$E_f = 28.8$
	$G_{ft} = 0.08$	$G_{ft} = 0.08$	$G_{ft} = 0.06$	$G_{ft} = 0.01$
Computed	$G_{tt} = 0.99$	$G_{tt} = 0.99$	$G_{tt} = 0.99$	$G_{tt} = 0.99$
	$G_c = 0.005$	$G_c = 0.005$	$G_c = 0.005$	$G_c = 0.005$
	$\nu_{tt} = 0.98$	$\nu_{tt} = 0.98$	$\nu_{tt} = 0.98$	$\nu_{tt} = 0.98$
Fixed	$E_t = 1$	$E_t = 1$	$E_t = 1$	$E_t = 1$
	$\nu_{ft} = 0.49$	$\nu_{ft} = 0.49$	$\nu_{ft} = 0.49$	$\nu_{ft} = 0.49$
	$E_c = 0.5$	$E_c = 0.5$	$E_c = 0.5$	$E_c = 0.5$
	$\nu_c = -0.99$	$\nu_c = -0.99$	$\nu_c = -0.99$	$\nu_c = -0.99$

Table 4: Quasi-incompressible cardiomyocyte and collagen optimized material parameter ratios (normalized by $E_t = 1$) in the laminar mesostructure (L), for β ranging between $\pm 0°, \pm 12.5°, \pm 25°$, and $\pm 50°$.

agreement between experiments and model, with a fair match starting from $\beta = \pm 25°$.

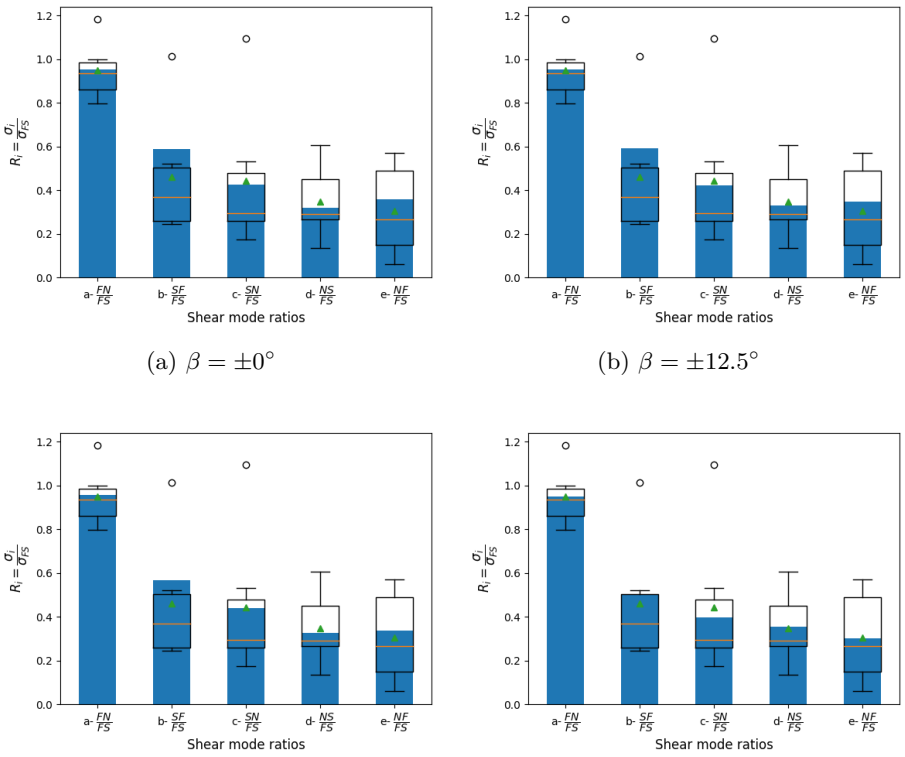

(a) $\beta = \pm 0°$ (b) $\beta = \pm 12.5°$

(c) $\beta = \pm 25°$ (d) $\beta = \pm 50°$

Figure 9: Compressible cardiomyocytes in the laminar mesostructure (L), for $\alpha = \pm 18°$, with β ranging between $\pm 0°$ (a), $\pm 12.5°$ (b), $\pm 25°$ (c), $\pm 50°$ (d).

3.3 Mesostructure (E)

Mesostructure (E) is made of aligned cardiomyocytes separated by an ellipsoidal layer of collagen. As for Mesostructure (L), we consider the effect of the sheetlet angle (β) variation within the macroscale cube.

Quasi-incompressible cardiomyocytes For quasi-incompressible cardiomyocytes, the experimental *vs.* numerical shear mode ratios are represented in Figure 10, for sheetlet angles β of $\pm 0°$ and $\pm 50°$. As for the previous mesostructure, using quasi-incompressible cardiomyocytes, the order and the values of the experimental ratios were not matched numerically, despite the in-

troduction of high angles of sheetlet rotations. We therefore conclude that the extra degree of freedom of compressibility is needed.

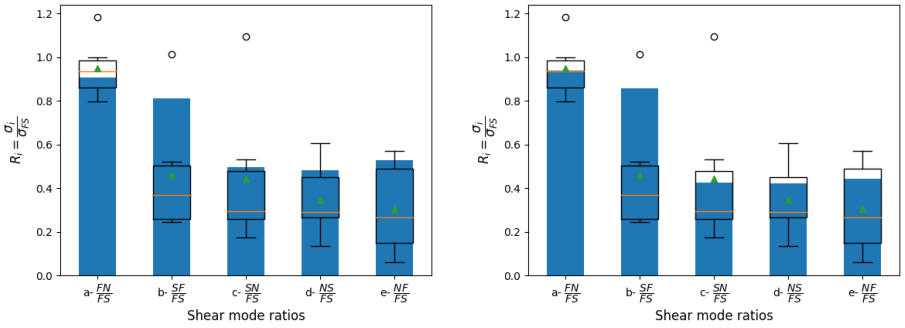

(a) $\beta = 0°$ (b) $\beta = 50°$

Figure 10: Quasi-incompressible cardiomyocyte in a circular cluster mesostructure (E), with $\beta = \pm 0°$ (a) and $\beta = \pm 50°$ (b).

Compressible cardiomyocytes The optimization results for mesostructure (E) with compressible cardiomyocytes are shown in Figure 11, for sheetlet angles β of $\pm 0°$ and $\pm 50°$. The results observed for this mesostructure were similar to the results of mesostructure (L): the observed anisotropy was able to be reproduced by rotating the sheetlets, and the solution was not unique.

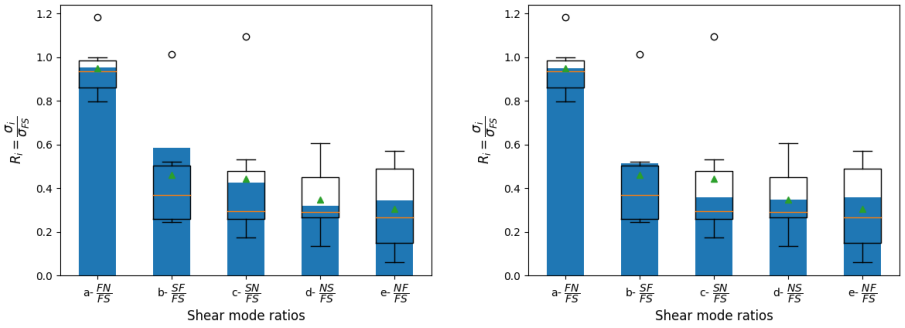

(a) $\beta = 0°$ (b) $\beta = 50°$

Figure 11: Compressible cardiomyocyte in a circular cluster mesostructure (E), with $\beta = \pm 0°$ (a) and $\beta = \pm 50°$ (b).

3.4 Size effect

The obtained results are shown in Figure 12. The curves for a mesostructure without sheetlet orientation variation show a quasi-constant evolution of the anisotropy with the cube size. The effect of the sheetlet orientation variation is shown in (b). The anisotropy is not conserved with the sample size, hinting at the presence of important size effects. While the anisotropy order is maintained for samples of $3\times3\times3$ mm^3 and $4\times4\times4$ mm^3, in agreement with the experimental observations [Dokos et al., 2002; Sommer et al., 2015] on samples of 3 mm and 4 mm respectively, we predict that the curves will intersect for samples larger than 5 mm, with an important increase of the shear stress in FN and NS.

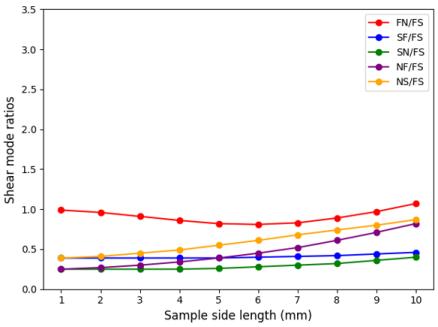

(a) Cardiomyocyte orientation.

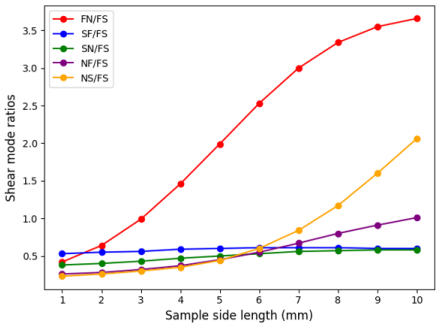

(b) Cardiomyocyte and sheetlet orientation.

Figure 12: Numerical shear stress ratios for samples ranging from 1 to 10 mm size, taking into account the cardiomyocyte orientation variation only (a), and the cardiomyocyte and sheetlet orientation variation (b).

4 Discussion

In this study, we investigated the microstructural origin of the anisotropic behavior of the cardiac tissue and we tested if it is solely induced by the rotation of the cardiomyocytes in the heart wall, or by the presence of collageneous extracellular layers at the mesoscale. We analyzed the macroscopic behavior of the cardiac tissue composed of different mesostructural configurations consisting in several organizations of cardiomyocytes and collagen planes. The orthotropic material behavior induced by these mesostructures was compared to stresses resulting from the application of shear displacement in six different modes on myocardial samples.

The experimental data provided by Prof. Socrates Dokos showed that the anisotropy is independent of the deformation level (see Figure 4), which allowed us to conduct our study for small deformations, in a linear elastic limit.

Our study also shows that it is not possible to reproduce the macroscopic

anisotropy with a transversely isotropic model, *i.e.*, by solely taking into account the transversely isotropic nature of the myocardium at the mesoscale, and the transmural variation of the fiber orientation (see Figure 7). Nonetheless, the consideration of the sheetlet structure at the mesoscale allows to replicate the macroscopic shear ratios (see Figures 9 & 11). This result is in accordance with a study performed by [Schmid et al., 2008], where macroscopic orthotropic compressible models are used to fit the macroscopic shear stresses from [Dokos et al., 2002]. Additionally, we show that the sheetlet orientation variation plays an important role in the anisotropy (see Figures 9 & 11), with a better agreement between numerical and experimental results for higher values of angle β. It is worth noting that important linear variations of this orientation were considered ($\pm 50^\circ$ in a $3\times3\times3$ mm cubic sample). This leads to an unrealistic variation of the sheetlet orientation of more than 300° in the cardiac wall, however, it served to evaluate the importance of these angles in the macroscopic anisotropy response. Conversely, other configurations, such as a non-linear transmural sheetlet orientation variation [Nielles-Vallespin et al., 2017], or the coexistence of two distinct sheetlet populations [Kilner et al., 2015], could potentially be investigated.

One essential assumption tested in this study is the incompressible behavior of myocardial constituents, mainly the block of cardiomyocytes surrounded by endomysial collagen (red blocks in Figure 2). The results show that this assumption does not allow to reproduce the observed macroscopic anisotropy for mesostructures (H), (L) and (E). We therefore suggest that the myocardium has a certain level of compressibility, with changes in volume occurring in the endomysial and perimysial extracellular matrices. Indeed, a microstructural model developed by [McEvoy et al., 2018] suggested that the myocardium should be considered as a slightly compressible material.

It is worth mentioning that, considering the compressibility hypothesis, and taking into account the microstructure orientation variation, we were not able to determine which of mesostructures (L) or (E) best reproduced the experimental results. To do so, more experimental data are required, at different scales, to better fit the results. Indeed, this study hinted at the presence of important size effects of the anisotropy, that should not be overlooked in numerical models. When the sheetlet structure is taken into account, the anisotropy increases with the increase of the the tissue sample sizes, and, more importantly, it is not maintained. While the FN shear stress mode is dominant for most tissue sizes, the response to shear in NS and NF increase in an unexpected way with the increase of the sample size.

At last, our study revealed several sets of parameters to fit the macroscopic data. Further sensitivity analysis should be performed to investigate the parameters influence on the macroscopic result. Moreover, a better understanding of the microscopic parameters would allow a finer definition of the parameter bounds, hence a better parameter optimization. This highlights the need for more multiscale experiments on cardiac tissue.

5 Conclusion

We proposed a multiscale model of the myocardium aiming at determining the structural origin of the observed macroscale mechanical anisotropy. Our study suggests that the cardiac anisotropy observed at the macroscale is not induced by large deformations, but is inherent to the tissue. Moreover, our results show the importance of the cardiac structure on its mechanical properties. Indeed, the macroscopic anisotropy is not only induced by the transmural rotation of the cardiomyocytes, but also by the organization and transmural rotation of collagen layers at the mesoscale. An additional finding is that some level of compressibility is required to fit the data. Furthermore, we highlighted important size effects that should be taken into consideration in cardiac models.

References

Martin Alnæs, Jan Blechta, Johan Hake, August Johansson, Benjamin Kehlet, Anders Logg, Chris Richardson, Johannes Ring, Marie E Rognes, and Garth N Wells. The FEniCS Project Version 1.5. *Archive of Numerical Software*, Vol 3, 2015. doi: 10.11588/ans.2015.100.20553.

H. Ashikaga, B.A. Coppola, K.G. Yamazaki, F.J Villarreal, J.H. Omens, and J.W. Covell. Changes in regional myocardial volume during the cardiac cycle: Implications for transmural blood flow and cardiac structure. *American Journal of Physiology-Heart and Circulatory Physiology*, 295(2):H610–H618, 2008. doi: 10.1152/ajpheart.00107.2008.

R. Avazmohammadi, MR. Hill, MA. Simon, W. Zhang, and M Sacks. A novel constitutive model for passive right ventricular myocardium: Evidence for myofiber–collagen fiber mechanical coupling. *Biomechanics and Modeling in Mechanobiology*, 16(2):561–581, 2017. doi: 10.1007/s10237-016-0837-7.

K.D. Costa, J. W. Holmes, and A. D. Mcculloch. Modelling cardiac mechanical properties in three dimensions. *Philosophical Transactions of the Royal Society of London. Series A: Mathematical, Physical and Engineering Sciences*, 359(1783):1233–1250, 2001. doi: 10.1098/rsta.2001.0828.

C.R.G. Debessa, L.B.M. Maifrino, and R.R. de Souza. Age related changes of the collagen network of the human heart. *Mechanisms of Ageing and Development*, pages 1049–1058, 2001. doi: 10.1016/s0047-6374(01)00238-x.

H. Demiray. Stresses in Ventricular Wall. *Journal of Applied Mechanics*, 43(2): 194–197, 1976. doi: 10.1115/1.3423806.

S. Dokos, B.H. Smaill, A.A. Young, and I.A. LeGrice. Shear properties of passive ventricular myocardium. *American Journal of Physiology-Heart and Circulatory Physiology*, 283(6):H2650–H2659, 2002. doi: 10.1152/ajpheart.00111.2002.

P.F. Ferreira, P.J. Kilner, L-A. McGill, S. Nielles-Vallespin, A.D. Scott, Siew Y Ho, Karen P McCarthy, Margarita M Haba, Tevfik F Ismail, Peter D Gatehouse, Ranil de Silva, Alexander R Lyon, Sanjay K Prasad, David N Firmin, and Dudley J Pennell. In vivo cardiovascular magnetic resonance diffusion tensor imaging shows evidence of abnormal myocardial laminar orientations and mobility in hypertrophic cardiomyopathy. *Journal of Cardiovascular Magnetic Resonance*, 16(1):87, 2014. doi: 10.1186/s12968-014-0087-8.

J. J. Garcia, N. J. Altiero, and R. C. Haut. An Approach for the Stress Analysis of Transversely Isotropic Biphasic Cartilage Under Impact Load. *Journal of Biomechanical Engineering*, 120(5):608–613, 1998. doi: 10.1115/1.2834751.

J. M. Guccione, A. D. McCulloch, and L. K. Waldman. Passive Material Properties of Intact Ventricular Myocardium Determined From a Cylindrical Model. *Journal of Biomechanical Engineering*, 113(1):42–55, 1991. doi: 10.1115/1.2894084.

R. Hill. Elastic properties of reinforced solids: Some theoretical principles. *Journal of the Mechanics and Physics of Solids*, 11(5):357–372, September 1963. doi: 10.1016/0022-5096(63)90036-x.

G.A. Holzapfel and R.W. Ogden. Constitutive modelling of passive myocardium: A structurally based framework for material characterization. *Philosophical Transactions of the Royal Society A: Mathematical, Physical and Engineering Sciences*, 367(1902):3445–3475, 2009. doi: 10.1098/rsta.2009.0091.

A. Horowitz, Y. Lanir, F. C. P. Yin, M. Perl, I. Sheinman, and R. K. Strumpf. Structural Three-Dimensional Constitutive Law for the Passive Myocardium. *Journal of Biomechanical Engineering*, 110(3):200–207, 1988. doi: 10.1115/1.3108431.

J. D. Humphrey and F. C. P. Yin. On Constitutive Relations and Finite Deformations of Passive Cardiac Tissue: I. A Pseudostrain-Energy Function. *Journal of Biomechanical Engineering*, 109(4):298–304, 1987. doi: 10.1115/1.3138684.

J.D. Humphrey and F.C.P. Yin. Biomechanical experiments on excised myocardium: Theoretical considerations. *Journal of Biomechanics*, 22(4):377–383, 1989. doi: 10.1016/0021-9290(89)90052-3.

P. J. Hunter. *Finite Element Analysis of Cardiac Muscle Mechanics.* PhD thesis, University of Oxford, 1975.

C. Igel, T. Suttorp, and N. Hansen. A computational efficient covariance matrix update and a (1+1)-CMA for evolution strategies. In *Proceedings of the 8th Annual Conference on Genetic and Evolutionary Computation - GECCO '06*, page 453, Seattle, Washington, USA, 2006. ACM Press. doi: 10.1145/1143997.1144082.

Y. Kanzaki, F. Terasaki, M. Okabe, S. Fujita, T. Katashima, K. Otsuka, and N. Ishizaka. Three-Dimensional Architecture of Cardiomyocytes and Connective Tissue in Human Heart Revealed by Scanning Electron Microscopy. *Circulation*, 122(19):1973–1974, 2010. doi: 10.1161/circulationaha.110.979815.

P.J. Kilner, K. McCarthy, M. Murillo, P. Ferreira, A.D. Scott, Laura-Ann McGill, Sonia Nielles-Vallespin, Ranil Silva, Dudley J Pennell, Siew Y Ho, and David Firmin. Histology of human myocardial laminar microstructure and consideration of its cyclic deformations with respect to interpretation of in vivo cardiac diffusion tensor imaging. *Journal of Cardiovascular Magnetic Resonance*, 17(S1):Q10, 2015. doi: 10.1186/1532-429x-17-s1-q10.

G.L. Kung, T.C. Nguyen, A. Itoh, S. Skare, N.B. Ingels, D.C. Miller, and D.B. Ennis. The presence of two local myocardial sheet populations confirmed by diffusion tensor MRI and histological validation. *Journal of Magnetic Resonance Imaging*, 34(5):1080–1091, 2011. doi: 10.1002/jmri.22725.

I. J. LeGrice, B. H. Smaill, L. Z. Chai, S. G. Edgar, J. B. Gavin, and P. J. Hunter. Laminar structure of the heart: Ventricular myocyte arrangement and connective tissue architecture in the dog. *American Journal of Physiology-Heart and Circulatory Physiology*, 269(2):H571–H582, 1995. doi: 10.1152/ajpheart.1995.269.2.h571.

B. M. Lempriere. Poisson's ratio in orthotropic materials. *AIAA Journal*, 6 (11):2226–2227, 1968. doi: 10.2514/3.4974.

A. Loredo and H. Klöcker. Generalized inverse of the compliance tensor, and behaviour of incompressible anisotropic materials — Application to damage. *Mechanics Research Communications*, 24(4):371–376, 1997. doi: 10.1016/S0093-6413(97)00038-4.

E. McEvoy, G.A. Holzapfel, and P. McGarry. Compressibility and Anisotropy of the Ventricular Myocardium: Experimental Analysis and Microstructural Modeling. *Journal of Biomechanical Engineering*, 140(8):081004, 2018. doi: 10.1115/1.4039947.

J.C. Michel, H. Moulinec, and P. Suquet. Effective properties of composite materials with periodic microstructure: A computational approach. *Computer Methods in Applied Mechanics and Engineering*, 172(1-4):109–143, 1999. doi: 10.1016/s0045-7825(98)00227-8.

S. Nielles-Vallespin, Z. Khalique, P.F. Ferreira, R. de Silva, A.D. Scott, P. Kilner, L.A. McGill, A. Giannakidis, P.D. Gatehouse, D. Ennis, E. Aliotta, M. Al-Khalil, P. Kellman, D. Mazilu, R.S. Balaban, D.N. Firmin, A.E. Arai, and D.J. Pennell. Assessment of Myocardial Microstructural Dynamics by In Vivo Diffusion Tensor Cardiac Magnetic Resonance. *Journal of the American College of Cardiology*, 69(6):661–676, 2017. doi: 10.1016/j.jacc.2016.11.051.

D.R. Nolan, A.L. Gower, M. Destrade, R.W. Ogden, and J.P. McGarry. A robust anisotropic hyperelastic formulation for the modelling of soft tissue. *Journal of the Mechanical Behavior of Biomedical Materials*, 39:48–60, 2014. doi: 10.1016/j.jmbbm.2014.06.016.

A.J. Pope, G.B. Sands, B.H. Smaill, and I.J. LeGrice. Three-dimensional transmural organization of perimysial collagen in the heart. *American Journal of Physiology-Heart and Circulatory Physiology*, 295(3):H1243–H1252, 2008. doi: 10.1152/ajpheart.00484.2008.

D. Rohmer, A. Sitek, and G.T. Gullberg. Reconstruction and Visualization of Fiber and Laminar Structure in the Normal Human Heart from Ex Vivo Diffusion Tensor Magnetic Resonance Imaging (DTMRI) Data:. *Investigative Radiology*, 42(11):777–789, 2007. doi: 10.1097/rli.0b013e3181238330.

E. Sanchez-Palencia. Comportements local et macroscopique d'un type de milieux physiques heterogenes. *International Journal of Engineering Science*, 12(4):331–351, 1974. doi: 10.1016/0020-7225(74)90062-7.

G.B. Sands, D.A. Gerneke, D.A. Hooks, C.R. Green, B.H. Smaill, and I.J. Legrice. Automated imaging of extended tissue volumes using confocal microscopy. *Microscopy Research and Technique*, 67(5):227–239, 2005. doi: 10.1002/jemt.20200.

H. Schmid, M. P. Nash, A. A. Young, and P. J. Hunter. Myocardial Material Parameter Estimation: A Comparative Study for Simple Shear. *Journal of Biomechanical Engineering*, 128(5):742–750, 2006. doi: 10.1115/1.2244576.

H. Schmid, P. O'Callaghan, M. P. Nash, W. Lin, I. J. LeGrice, B. H. Smaill, A. A. Young, and P. J. Hunter. Myocardial material parameter estimation: A non–homogeneous finite element study from simple shear tests. *Biomechanics and Modeling in Mechanobiology*, 7(3):161–173, 2008. doi: 10.1007/s10237-007-0083-0.

G. Sommer, A..J. Schriefl, M. Andrä, M. Sacherer, C. Viertler, H. Wolinski, and G.A. Holzapfel. Biomechanical properties and microstructure of human ventricular myocardium. *Acta Biomaterialia*, 24:172–192, 2015. doi: 10.1016/j.actbio.2015.06.031.

D.D. Streeter and D.L. Bassett. An engineering analysis of myocardial fiber orientation in pig's left ventricle in systole. *The Anatomical Record*, 155(4): 503–511, 1966. doi: 10.1002/ar.1091550403.

D.D. Streeter, H.M. Spotnitz, D.P. Patel, J. Ross, and E.H. Sonnenblick. Fiber Orientation in the Canine Left Ventricle during Diastole and Systole. *Circulation Research*, 24(3):339–347, 1969. doi: 10.1161/01.res.24.3.339.

A.A. Young, I.J. Legrice, M.A. Young, and B.H. Smaill. Extended confocal microscopy of myocardial laminae and collagen network. *Journal of Microscopy*, 192(2):139–150, 1998. doi: 10.1046/j.1365-2818.1998.00414.x.

Supplementary information

A Comparison of experimental shear stress studies

The results of [Dokos et al., 2002] reveal the material's anisotropy with the difference in the shear stresses along the six directions, with the highest values for the FS and FN modes, and the lowest ones for the NF and NS modes.

Similar results were also found in a more recent study on human hearts [Sommer et al., 2015]. In Figure 13, we plotted the peak stress values at 50% deformation for both studies. The detailed data provided by Prof. Socrates Dokos allowed us to plot the dispersion, however, we did not have the data from the second study. We thus used the published experimental results. Although the peak shear stress values obtained for swine are higher than the ones obtained for humans, the ratios of the modes over SF are similar, with a slight difference in modes NS and NF (see Figure 13). However, these modes seem to be interchangeable in the literature, with no significant difference found between them [Dokos et al., 2002; Sommer et al., 2015; McEvoy et al., 2018].

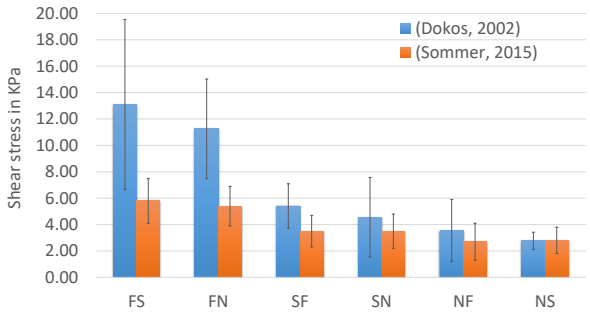

Figure 13: Comparison of experimental data extracted from [Dokos et al., 2002] and [Sommer et al., 2015]. Bar plot of the peak shear stress values for 50% deformation for both studies. The stress values recorded in [Dokos et al., 2002], performed on swine hearts, are higher than the ones recorded in [Sommer et al., 2015], performed on human hearts. However, the order of the modes is similar with FS>FN≥SF>SN>NF≅NS.

Using the data from [Dokos et al., 2002], we plotted the recorded peak stress of each mode, at 5% deformation for the four cycles (see Figure 14). At the first cycle, the anisotropy is evident, with high shear stresses for modes FS and FN (≅ 0.6 kPa), followed by SF and SN (≅ 0.3 Kpa), and low stresses for NS and NF (≅ 0.2 kPa). We noticed that the stresses tended to converge with the cycles, reaching ≅ 0.02 kPa for all modes. This means that the more cycles the tissue is subjected to, the more it is preconditioned, the more is loses of its anisotropy and becomes isotropic. We thus decided to study the small

deformation anisotropy at the first cycle.

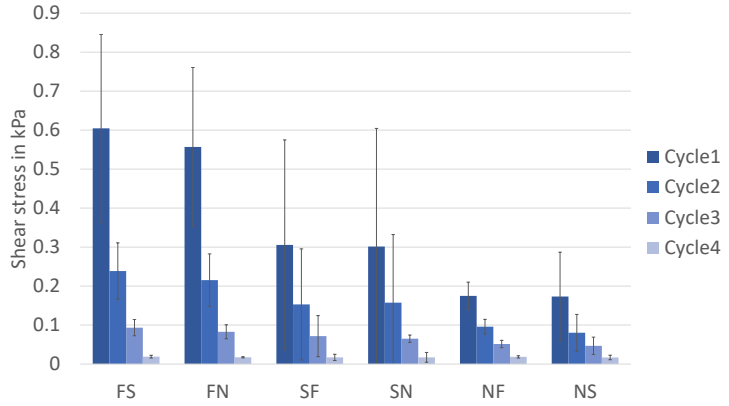

Figure 14: Comparison of the peak shear stress recorded at 5% deformation for all cycles. Cycle 1 shows clear anisotropy with high shear stresses for modes FS and FN, and low stresses for NS and NF. Shear stress decreases with cycles, and reaches a same amplitude for all modes at cycle 4. Data extracted from [Dokos et al., 2002].

Given that our main objective was to compare the anisotropy, hence the order of the shear stresses, we computed the experimental ratios over FS, FS corresponding to the mode with the highest recorded shear stresses. This also required to fix one of the material parameters, therefore reducing the number of parameters to optimize.

B Sensitivity analysis

In principle, the estimation of microscopic parameters from macroscopic experimental data is an ill-posed problem. We thus needed to characterize the material parameters identifiability before the actual parameter optimization. The sensitivity analysis was performed at two scales, using synthetic data generated with the model. We studied the material parameters influence on the homogenized stiffness matrix at the mesoscale, and on the shear stresses at the macroscale. This was performed by evaluating the Hessian matrix of the cost function using finite differences. In order to obtain a non-dimensional matrix, we introduced the non-dimensional parameter $\underline{\bar{p}}$ such that:

$$\underline{\bar{p}} = (\underline{p} - \underline{p_0}) \oslash \underline{p_0}, \tag{B.1}$$

$\underline{p_0}$ being a reference value of the parameters, and $\oslash$ the Hadamard division.

The non-dimensional stiffness matrix cost function $\bar{J}$ is defined such that:

$$\bar{J}(\underline{\bar{p}}) = J(\underline{p} = \underline{p_0} \odot (\underline{1} + \underline{\bar{p}})), \tag{B.2}$$

with $\odot$ the Hadamard product.

Using $\bar{J}(\bar{p})$, the first derivative $\nabla \bar{J}$ could thus be computed such that:

$$\nabla \bar{J}_i = \frac{\bar{J}(\underline{\bar{p}} + \bar{h}_i \underline{\bar{e}_i}) - \bar{J}(\underline{\bar{p}})}{\bar{h}_i}, \tag{B.3}$$

and the hessian such that:

$$\nabla^2 \bar{J}_{ij} = \frac{\bar{J}(\underline{\bar{p}} + \bar{h}_i \underline{\bar{e}_i} + \bar{h}_j \underline{\bar{e}_j}) - \bar{f}(\underline{\bar{p}} + \bar{h}_i \underline{\bar{e}_i}) - \bar{f}(\underline{\bar{p}} + \bar{h}_j \underline{\bar{e}_j}) + \bar{f}(\underline{\bar{p}})}{\bar{h}_i \bar{h}_j}, \tag{B.4}$$

where $\bar{h}_i$ and $\bar{h}_j$ are the introduced perturbations in the $\underline{\bar{e}_i}$ and $\underline{\bar{e}_j}$ directions, typically equal to 10^{-6} *a.u.*

Sensitivity of the homogenized stiffness matrix to microscopic parameters. At the mesoscale, we used the material parameters as an input and computed a homogenized stiffness matrix. We therefore studied the sensitivity of the homogenized matrix on the material parameters $\underline{p}$, by evaluating the Hessian matrix in Equation (B.4), with the error $\bar{J}(\underline{\bar{p}}) = \bar{\bar{J}}_m(\underline{\bar{p}})$ computed such that:

$$\bar{J}_m = \sum_{n=1}^{N_\lambda} \frac{(\lambda_i' - \lambda_i)^2}{\lambda_i^2}, \tag{B.5}$$

with λ_i and λ_i' being respectively the eigenvalues of the stiffness matrix and the perturbed stiffness matrix and $N_\lambda = 6$.

The analysis was performed on mesostructures H, L and E, with compressible cardiomyocytes (presented first), and quasi-incompressible cardiomyocytes (presented next).

In the case of the compressible homogeneous mesostructure (H), with four parameters, E_f, G_{ft}, ν_{ft} and ν_{tt}, with $E_t = 1$ *a.u.* being fixed since only the shear stress ratios are considered, Table 5 shows that parameters E_f, G_{ft} and ν_{tt} are associated with positive eigenvalues. The homogenized stiffness matrix is thus sensitive to these parameters. However, ν_{ft} is associated with a near-zero eigenvalue. Therefore, at the mesoscale, ν_{ft} has no or little impact on the homogenized stiffness matrix.

For mesostructures L and E, six input parameters were investigated, considering a compressible transversely isotropic material for cardiomyocytes and an isotropic material for the perimysial extracellular matrix. The cardiomyocyte parameters are $\underline{p}_{cells} = \{E_f, E_t, G_{ft}, G_{tt}, \nu_{ft}, \nu_{tt}\}$, where $E_t = 1$ *a.u.* is fixed and $G_{tt} = \frac{E_t}{2(1+\nu_{tt})}$. The collagen parameters are $\underline{p}_{ECM} = \{E_c, G_{cp}, \nu_c\}$, where $G_{cp} = \frac{E_c}{2(1+\nu_p)}$. The Hessian matrix eigenvalues and relative eigenvectors were computed. The primary directions of the eigenvectors relative to parameters ν_c, E_c and ν_{ft} (see Tables 6 and 7) are associated with small eigenvalues. A small variation of these parameters has therefore no or very little impact on the homogenized stiffness matrix. These parameters are associated with the perimysial extracellular matrix (except for ν_{ft}), which can be explained by the fact that the extracellular matrix layer is thin, and represents only 5% of the

Eigenvalues				
4.00	2.00	0.06	**0.00**	
Eigenvectors				
0.00	+1.00	0.00	0.00	E_f
+1.00	0.00	0.00	0.00	G_{ft}
0.00	0.00	0.00	-1.00	ν_{ft}
0.00	0.00	-1.00	0.00	ν_{tt}

Table 5: Eigenvalues and associated eigenvectors of the Hessian computing the sensitivity of the homogenized material matrix to microscopic parameters in the isotropic compressible case. Red indicates the parameter corresponding to the principle direction relative to the eigenvalue.

total volume. The choice of an isotropic material for the perimysial layer with less material parameters is thus suitable.

Eigenvalues						
18.50	3.63	1.96	0.01	**0.00**	**0.00**	
Eigenvectors						
0.00	0.00	+1.00	0.00	0.00	0.00	E_f
0.00	+1.00	0.00	0.00	0.00	0.00	G_{ft}
0.00	0.00	0.00	0.00	0.00	-1.00	ν_{ft}
-1.00	0.00	0.00	0.00	0.00	0.00	ν_{tt}
0.00	0.00	0.00	+1.00	0.00	0.00	E_c
0.00	0.00	0.00	+0.08	+1.00	0.00	ν_c

Table 6: Eigenvalues and associated eigenvectors of the Hessian computing the sensitivity of the homogenized material matrix to microscopic parameters for mesostructure L with compressible cardiomyocytes. Red indicates the parameter corresponding to the principle direction relative to the eigenvalue.

In the case of the homogeneous mesostructure (H) with quasi-incompressible cardiomyocytes, two parameters E_f and G_{ft} are investigated, $E_t = 1$ $a.u.$ being fixed since the ratios are studied. At the mesoscale, Table 8 shows that both parameters E_f and G_{ft} have eigenvectors associated with positive eigenvalues. The homogenized material matrix is thus sensitive to both.

For the laminar (L) and elliptical (E) mesostructures with quasi-incompressible cardiomyocytes, two parameters E_f and G_{ft} corresponding to the cardiomyocytes, and parameters E_c and ν_{cp} corresponding to the perimysial extracellular matrix are investigated.

Table 9 shows that the homogenized stiffness matrix is sensitive to parameters E_f, G_{ft} and E_c.

Mesostructure (E) shows the same parameter sensitivity results as mesostructure (L), with no sensitivity for parameter ν_{cp} at the mesoscale.

Eigenvalues						
60.20	3.57	0.16	0.01	**0.00**	**0.00**	
Eigenvectors						
-0.11	0.00	+0.79	-0.33	+0.50	-0.04	E_f
0.00	+1.00	0.00	0.00	0.00	0.00	G_{ft}
0.00	0.00	+0.60	+0.44	-0.67	-0.01	ν_{ft}
-0.99	0.00	-0.09	+0.06	-0.04	0.00	ν_{tt}
-0.02	0.00	0.00	-0.83	-0.55	+0.09	E_c
0.00	0.00	+0.03	+0.06	+0.06	+1.00	ν_c

Table 7: Eigenvalues and associated eigenvectors of the Hessian computing the sensitivity of the homogenized material matrix to microscopic parameters for mesostructure E with compressible cardiomyocytes. Red indicates the parameter corresponding to the principle direction relative to the eigenvalue.

Eigenvalues		
4.00	4.00	
Eigenvectors		
+1.00	0.00	E_f
0.00	+1.00	G_{ft}

Table 8: Eigenvalues and associated eigenvectors of the Hessian computing the sensitivity of the homogenized material matrix to microscopic parameters in the isotropic quasi-incompressible case. Red indicates the parameter corresponding to the principle direction relative to the eigenvalue.

Eigenvalues				
3.71	2.08	0.83	**0.00**	
Eigenvectors				
+0.04	+0.94	+0.34	0.00	E_f
+1.00	-0.06	+0.07	+0.01	G_{ft}
+0.08	+0.33	-0.94	-0.05	E_c
0.00	+0.02	-0.05	+1.00	ν_{cp}

Table 9: Eigenvalues and associated eigenvectors of the Hessian computing the sensitivity of the homogenized material matrix to microscopic parameters for mesostructure L with incompressible cardiomyocytes. Red indicates the parameter corresponding to the principle direction relative to the eigenvalue.

Eigenvalues				
3.29	1.90	0.56	**0.00**	
Eigenvectors				
+0.09	+0.86	+0.50	+0.02	E_f
+0.97	-0.19	+0.14	+0.02	G_{ft}
+0.21	+0.47	-0.85	-0.06	E_c
-0.01	+0.02	-0.07	+1.00	ν_{cp}

Table 10: Eigenvalues and associated eigenvectors of the Hessian computing the sensitivity of the homogenized material matrix to microscopic parameters for mesostructure E with incompressible cardiomyocytes. Red indicates the parameter corresponding to the principle direction relative to the eigenvalue.

Sensitivity of shear stresses to microscopic parameters. At the macroscale, the input parameter was the homogenized stiffness matrix and the outputs were the shear stresses. We therefore studied the influence of small variations of material parameters on the resulting shear stress via the homogenized stiffness matrix, by evaluating the hessian matrix in Equation (B.4), with $\bar{J}(\underline{\bar{p}}) = \bar{J}_M(\underline{\bar{p}})$ such that:

$$\bar{J}_M = \sum_{i=1}^{N_R} \frac{(R_i' - R_i)^2}{R_i^2} \tag{B.6}$$

with $N_R = 5$, the number of ratios to optimize. R_i are the ratios of the exact problem, and R_i' the ratios resulting from the problem with the perturbed parameters. At this scale, the three mesostructures H, L and E were investigated.

For mesostructure H, with compressible cardiomyocytes, four parameters E_f, G_{ft}, ν_{ft} and ν_{tt} were analyzed. The sensitivity analysis at the macroscale showed that the macroscopic response is not affected by the parameter ν_{ft}, hence ν_{ft} is not identifiable (see Table 11). This result was expected given that ν_{ft} has no impact on the homogenized matrix, as seen in the previous section. The rest of the parameters were associated with positive eigenvalues.

Eigenvalues				
1.80	0.47	0.03	**0.00**	
Eigenvectors				
0.00	0.00	-1.00	0.00	E_f
-0.11	-0.99	0.00	0.00	G_{ft}
0.00	0.00	0.00	+1.00	ν_{ft}
+0.99	-0.11	0.00	0.00	ν_{tt}

Table 11: Eigenvalues and associated eigenvectors of the Hessian computing the sensitivity of the shear stress to microscopic parameters in the isotropic compressible mesostructure. Red indicates the parameter corresponding to the principle direction relative to the eigenvalue.

For mesostructures L and E, we show here the sensitivity study for the case

with compressible cardiomyocytes. The analysis shows, again, that the extracellular matrix parameters are not identifiable, with a quasi-null sensitivity (see Tables 12 and 13). Thus, by performing simple shear assays at the macroscale, it is not possible to identify the non-sensitive parameters, mainly the extracellular matrix ones. This confirms our choice of reducing the number of parameters to identify for the extracellular matrix by choosing an isotropic material.

Eigenvalues						
0.63	0.32	0.03	**0.00**	**0.00**	**0.00**	
Eigenvectors						
+0.08	+0.03	+0.99	-0.05	+0.03	+0.02	E_f
+0.98	+0.19	-0.09	+0.04	-0.01	0.00	G_{ft}
0.00	0.00	-0.04	+0.01	+0.85	+0.53	ν_{ft}
+0.20	-0.98	+0.02	-0.04	+0.01	0.00	ν_{tt}
-0.03	-0.05	+0.05	+0.99	-0.05	+0.08	E_c
0.00	0.00	0.00	-0.09	-0.53	+0.84	ν_c

Table 12: Eigenvalues and associated eigenvectors of the Hessian computing the sensitivity of the shear stress to microscopic parameters in mesostructure L with compressible cardiomyocytes. Red indicates the parameter corresponding to the principle direction relative to the eigenvalue.

Eigenvalues						
0.54	0.27	0.02	**0.00**	**0.00**	**0.00**	
Eigenvectors						
+0.09	+0.06	+0.98	-0.17	+0.04	+0.01	E_f
+0.97	+0.20	-0.09	+0.05	-0.01	0.00	G_{ft}
0.00	0.00	-0.04	+0.01	+0.91	+0.41	ν_{ft}
+0.21	-0.98	+0.03	-0.06	+0.01	0.00	ν_{tt}
-0.02	-0.06	+0.17	+0.98	-0.03	+0.06	E_c
0.00	0.00	-0.01	-0.07	-0.41	+0.91	ν_c

Table 13: Eigenvalues and associated eigenvectors of the Hessian computing the sensitivity of the shear stress to microscopic parameters in mesostructure E with compressible cardiomyocytes. Red indicates the parameter corresponding to the principle direction relative to the eigenvalue.

In the case of incompressible cardiomyocytes, the macroscopic shear stress sensitivity to the microscopic material parameters is shown in Tables 14, 15 and 16.

At the macroscale, Table 14 shows that both parameters E_f and G_{ft} have eigenvectors associated with positive eigenvalues. The macroscopic shear stress is thus sensitive to both, in the case of the homogeneous mesostructure with incompressible cardiomyocytes.

Eigenvalues		
0.96	0.16	
Eigenvectors		
+0.26	-0.97	E_f
-0.97	+0.26	G_{ft}

Table 14: Eigenvalues and associated eigenvectors of the Hessian computing the sensitivity of the shear stress to microscopic parameters in the isotropic quasi-incompressible mesostructure. Red indicates the parameter corresponding to the principle direction relative to the eigenvalue.

Eigenvalues				
0.62	0.03	**0.00**	**0.00**	
Eigenvectors				
0.00	-1.00	0.00	0.00	E_f
-1.00	0.00	-0.00	0.00	G_{ft}
0.00	-0.00	-1.00	0.00	E_c
0.00	+0.01	0.00	+1.00	ν_{cp}

Table 15: Eigenvalues and associated eigenvectors of the Hessian computing the sensitivity of the shear stress to microscopic parameters in mesostructure L with incompressible cardiomyocytes. Red indicates the parameter corresponding to the principle direction relative to the eigenvalue.

Eigenvalues				
0.54	0.02	**0.00**	**0.00**	
Eigenvectors				
-0.08	-0.98	+0.18	+0.01	E_f
-1.00	+0.07	-0.05	0.00	G_{ft}
+0.03	-0.18	-0.98	+0.04	E_c
0.00	+0.01	+0.04	+1.00	ν_{cp}

Table 16: Eigenvalues and associated eigenvectors of the Hessian computing the sensitivity of the shear stress to microscopic parameters in mesostructure E with incompressible cardiomyocytes. Red indicates the parameter corresponding to the principle direction relative to the eigenvalue.

At the macroscale, in the case of mesostructures (L) and (E) with incompressible transversely isotropic cardiomyocytes and isotropic collagen layer, Tables 15 and 16 show that only the cardiomyocyte parameters E_f and G_{ft} can be identified with macroscopic mechanical tests, E_c and ν_{cp} being associated with quasi-null eigenvalues.